JOURNAL OF GEOPHYSICAL RESEARCH, VOL. 94, NO. D3, PAGES 3365–3375, MARCH 20, 1989

# Theoretical Algorithms for Satellite-Derived Sea Surface Temperatures

I. J. BARTON,[1] A. M. ZAVODY,[2] D. M. O'BRIEN,[1] D. R. CUTTEN,[3] R. W. SAUNDERS,[4] AND D. T. LLEWELLYN-JONES[2]

Reliable climate forecasting using numerical models of the ocean-atmosphere system requires accurate data sets of sea surface temperature (SST) and surface wind stress. Global sets of these data will be supplied by the instruments to fly on the ERS 1 satellite in 1990. One of these instruments, the Along-Track Scanning Radiometer (ATSR), has been specifically designed to provide SST in cloud-free areas with an accuracy of 0.3 K. The expected capabilities of the ATSR can be assessed using transmission models of infrared radiative transfer through the atmosphere. The performances of several different models are compared by estimating the infrared brightness temperatures measured by the NOAA 9 AVHRR for three standard atmospheres. Of these, a computationally quick spectral band model is used to derive typical AVHRR and ATSR SST algorithms in the form of linear equations. These algorithms show that a low-noise 3.7-$\mu$m channel is required to give the best satellite-derived SST and that the design accuracy of the ATSR is likely to be achievable. The inclusion of extra water vapor information in the analysis did not improve the accuracy of multiwavelength SST algorithms, but some improvement was noted with the multiangle technique. Further modeling is required with atmospheric data that include both aerosol variations and abnormal vertical profiles of water vapor and temperature.

## 1. INTRODUCTION

Recent climatic events, such as the 1982–1983 El Niño, and forecasts related to the effects of increasing atmospheric carbon dioxide and possible nuclear wars have resulted in a large increase in the use of climate models. In the past these models have been rather limited, in that they do not adequately describe the interaction between the Earth's atmosphere and oceans. As a result, numerical modelers of climate are now combining atmospheric and oceanic models in an attempt to better understand the vagaries of our global climate. The coupling of these two regimes is obviously at the sea surface, and the two parameters of major importance in the exchange of energy between the oceans and the atmosphere are the sea surface temperature (SST) and the surface wind speed. These two parameters can be measured from space, using infrared and microwave remote sensing. The international Tropical Ocean Global Atmosphere (TOGA) program has specified accuracies of 0.3 K and 0.5 m $s^{-1}$, respectively, as requirements for global numerical models of climate. The current operational meteorological satellites do not obtain these accuracies; in fact, wind speed has not been available from space on an operational basis since the demise of Seasat in 1978. The AVHRR instruments on the NOAA satellites can supply SST in cloud-free areas, with an accuracy of 0.7 K in mid-latitudes and a somewhat poorer accuracy in tropical regions where moist atmospheres absorb much of the surface-emitted infrared radiation [*Barton*, 1983]. It is important to note that all of the algorithms discussed in this paper relate to cloud-free conditions and are derived with a fixed aerosol content. The detection of cloud-contaminated pixels, the derivation of SST from partly cloudy data, and the errors introduced by various clouds are the topics of several recent papers (see, for example, *Saunders and Kriebel* [1988] and references therein).

The ERS 1 satellite, to be launched by the European Space Agency in 1990, is expected to supply climate modelers with accurate satellite-derived sea surface data for use in ocean-atmosphere models. The surface wind speed and sea state will be monitored with both the Radar Altimeter and the Active Microwave Instrumentation (wind scatterometer and synthetic aperture radar). Surface wind speed will be measured by both instruments, with an accuracy of better than 2 m $s^{-1}$. The ERS 1 satellite will also carry the Along-Track Scanning Radiometer (ATSR), which is a new generation infrared and microwave radiometer that has been specifically designed to measure SST from space with the accuracy required by the TOGA program. This instrument operates at the same wavelengths as the AVHRR (namely, 3.7, 10.8, and 12.0 $\mu$m) and includes active cooling of the detectors, improved on-board calibration, a dual-angle view of the sea surface, and two passive microwave channels to obtain the total water vapor content of the atmosphere beneath the satellite. The derivation of operational algorithms to supply the accurate SSTs from the ATSR data is a task that requires much care. Theoretical models of infrared transmission through the atmosphere can be used to derive prelaunch algorithms, to select which algorithm is best suited to a particular geographic location or time of day, and to make some estimate of the final accuracy of the SST product. These models can also be used to determine an optimal form of SST retrieval algorithm for the ATSR data.

As with the operational Multi-Channel SST (MCSST) provided by the National Oceanic and Atmospheric Administration (NOAA) National Environmental Satellite, Data, and Information Service (NESDIS) [*McClain et al.*, 1985], the prelaunch SST algorithms for ATSR will require some fine tuning after launch. The accuracy of the transmission models is still limited by the uncertainty in the water vapor continuum absorption coefficients in the thermal infrared band. Intensive

[1]Division of Atmospheric Research, CSIRO, Aspendale, Victoria, Australia.
[2]Rutherford Appleton Laboratory, Chilton, Oxford, England.
[3]Defence Science and Technology Organisation, Salisbury, South Australia, Australia.
[4]Meteorological Office Unit, Clarendon Laboratory, Oxford, England.



Paper number 88JD04176.
0148-0227/89/88JD04176$05.00

geophysical validation campaigns are planned to follow the launch of ERS 1 immediately, so that an accurate SST data set will be available early in the ERS 1 mission.

In this paper we build on the early work of *Deschamps and Phulpin* [1980] and others and investigate the differential absorption techniques used to account for the atmospheric absorption of surface-emitted infrared radiation. Initially, we compare the performance of several different atmospheric transmission models at the AVHRR and ATSR wavelengths. Then, a spectral band model, which performs as well as the other models and is computationally quicker, is used to derive some preliminary prelaunch SST algorithms for the ATSR. The performance of the different algorithms is discussed. The selection of models for this paper is by no means exhaustive; for instance, a parametric model based on line-by-line calculations may be faster and more accurate than the band model.

## 2. TRANSMISSION MODELS

The transmission models described in this section are later intercompared by calculating the satellite brightness temperatures in the thermal infrared channels that would be measured by the AVHRR instrument on the NOAA 9 operational satellite.

### 2.1. *LOWTRAN-6*

Details of the LOWTRAN-6 computer code are given by *Kneizys et al.* [1983]. This model computes both radiance and transmittance for a given atmospheric path at a moderate resolution (20 $cm^{-1}$), using a single parameter band model for the molecular absorption. A choice of atmospheres can be made from six predefined atmospheres (three of which were used in these calculations), or a user-defined atmosphere, and a number of aerosol models. In its original form, LOWTRAN-6 only computes radiance in one direction at a time. Hence for this application the surface radiance calculation was modified to combine the reflected downward radiance at the surface with the surface emission. Also, the original LOWTRAN zero-order aerosol scattering algorithm was replaced by the conservative aerosol scattering algorithm where scattered radiation is conserved [*Ben-Shalom et al.*, 1980]. The sea surface emissivity values were calcualted in the same manner as described in section 2.3. Emissivities were obtained for the midband wavelength and assumed constant over that band.

The water vapor continuum expression in the 700–1500 $cm^{-1}$ spectral region included a correction which has already been put into the FASCOD line-by-line model [*Clough*, 1986]. This change to the LOWTRAN-6 code results from a recent revision of the water continuum coefficients, which showed some overestimation of the absorption in this spectral region [*Burch and Alt*, 1984; *Cutten*, 1985]. It should also be noted that the expression in the original LOWTRAN-6 code differs from the one used in the spectral band model: that expression being the same as used in LOWTRAN-5 and earlier codes.

Aerosol extinction calculations were based upon the maritime model, with a ground-based visibility of 23 km for the first 2 km, the tropospheric aerosol model for the 2- to 10-km height range, and the background stratospheric aerosol model for 10–30 km.

### 2.2. *Line-by-Line Model*

The line-by-line model is described by *Llewellyn-Jones et al.* [1984] in their comparison between ship and satellite-derived SSTs in the North Atlantic. (The sources of data, atmospheric constituents considered, etc., are given in their Table 1.)

### 2.3. *Band Model*

The spectral band model calculates the brightness temperatures measured by a satellite instrument viewing the Earth's surface through the infrared windows of the atmosphere. The spectral resolution of the model is 20 $cm^{-1}$, and the absorption coefficients are based on those given by *Kneizys et al.* [1980] in the LOWTRAN-5 computer code, with the following variations.

Transmittances due to the uniformly mixed gases are obtained using the transmittance function given in the LOWTRAN-5 code and a scaled absorber amount using the equation of *Weinreb and Hill* [1980]. The absorption due to nitrogen in the 3.5- to 4.0-$\mu$m window that is not included in LOWTRAN-5 is also included and is based on the work of *Weinreb and Hill* [1980].

The effects of aerosol absorption are included in the transmission model by assuming a simple exponential distribution with a scale height of 1 km. The aerosol absorption coefficients are based on the values given by *Shettle and Fenn* [1979] for a maritime atmosphere, with a relative humidity of 90%.

For each spectral interval (20 $cm^{-1}$) the transmittance from the bottom of each layer to the satellite is calculated as the product of four transmittances; namely, water vapor lines, water vapor continuum, mixed gases (including nitrogen), and aerosols. The transmittance of each layer is specified as the ratio of the transmittances to the satellite from the bottom and the top of the layer.

The sea surface emissivity is calculated using Fresnel reflection coefficients and the complex refractive indices reported by *Pontier and Dechambenoy* [1966]. At normal incidence the emissivity values range between 0.97 and 0.98 for the 3.7-$\mu$m window and between 0.98 and 0.99 for the 10.3- to 12.5-$\mu$m region. At 60° incidence angle the emissivity ranges decrease to 0.93–0.94 and 0.93–0.97, respectively. The calculated values agree well with the recent tables published by *Masuda et al.* [1988]. Also, the emissivity values obtained near 11 $\mu$m are in good agreement with the aircraft measurements of *Saunders* [1967, 1968], which show that the emissivity is independent of sea state for incidence angles smaller than 60°. By assuming that the surface emissivity is nonunity, it is necessary to include the surface reflectance of downcoming sky radiation in the radiation upwelling from the surface. Specular reflection at the sea surface of the downcoming sky radiation is assumed.

To compute the satellite brightness temperatures, the model requires a specification of the sea surface temperature and the vertical profiles of temperature and water vapor content. Either radiosonde or standard atmosphere data are entered at significant levels, and the atmosphere between adjacent levels is subdivided into 10 layers of equal (height) thickness. The temperature of each layer is determined assuming a linear lapse rate and the pressure and water vapor content (partial pressure) determined assuming an exponential decrease with height. For radiosonde data a standard atmosphere is assumed between the uppermost level and 50 hPa, and no absorption is assumed above 50 hPa.

Starting at the top of the atmosphere, the model uses a recursive procedure to calculate the downcoming radiance at sea level and then adds the reflected component to the emitted radiation before repeating the recursive procedure in going from the surface to space. Further details of this technique are given by *Barton* [1985].

TABLE 1. Temperature Deficits for LOWTRAN, Line-by-Line, Spectral Band, and GENLN2 Models for the Three Standard Atmospheres of *McClatchey et al.* [1972]

| | | Zenith Angle = 0° | | | Zenith Angle = 50° | | |
|---|---|---|---|---|---|---|---|
| | Model | Tropical | MLS | MLW | Tropical | MLS | MLW |
| 3.7 μm | LWT | 3.54 | 2.64 | 1.49 | 4.82 | 3.62 | 2.14 |
| | LBL | 3.64 | 2.56 | 1.47 | 5.13 | 3.62 | 2.16 |
| | BND | 3.23 | 2.52 | 1.42 | 4.34 | 3.40 | 2.02 |
| | GL2* | 3.42 | 2.70 | 1.68 | 4.87 | 3.91 | 2.51 |
| 10.8 μm | LWT | 4.83 | 3.02 | 1.58 | 6.89 | 4.45 | 2.47 |
| | LBL | 4.13 | 2.38 | 0.96 | 5.78 | 3.45 | 1.64 |
| | BND | 4.29 | 2.53 | 1.11 | 5.96 | 3.60 | 1.74 |
| | GL2 | 3.95 | 2.32 | 0.84 | 5.61 | 3.38 | 1.44 |
| 12.0 μm | LWT | 5.95 | 3.51 | 1.28 | 8.18 | 4.83 | 2.06 |
| | LBL | 5.72 | 3.35 | 1.35 | 7.62 | 4.60 | 2.22 |
| | BND | 5.67 | 3.32 | 1.34 | 7.61 | 4.58 | 2.12 |
| | GL2 | 5.55 | 3.30 | 1.19 | 7.50 | 4.63 | 2.03 |

LWT, LOWTRAN; LBL, line-by-line; BND, spectral band; GL2, GENLN2; MLS, mid-latitude summer; MLW, mid-latitude winter.
*A deficit of 0.18 K for 0° and 0.28 K for 50° (the BND model values) was added for aerosols. No aerosols were included for the 10.8- and 12.0-μm channels.

### 2.4. *GENLN2*

Details of the latest line-by-line atmospheric transmission/radiance model under development at Oxford University are described by *Edwards* [1987, 1988]. For this particular application of computing AVHRR radiances using the model, the procedure and parameters outlined in the following paragraph were used.

The atmosphere was divided up into 30 layers, the lowest kilometer in 0.1-km layers, the next kilometer in 0.2-km layers and then in 0.5-km layers up to 6 km, 1-km layers up to 10 km, and then a 2-km, 13-km, and 25-km layer up to 50 km above the surface. Absorption above this altitude was neglected. The line data was taken from the 1986 AFGL line data base [*Rothman et al.*, 1987]. For AVHRR channel 3 (3.7 μm), absorption lines from the following gases were included in the calculation: $H_2O$, $CO_2$, $O_3$, $H_2CO$, $N_2O$, and $CH_4$. In addition, continuum absorption for $H_2O$, $CO_2$, and $N_2$ were also included. For AVHRR channels 4 (10.8 μm) and 5 (12 μm) absorption lines from $H_2O$, $CO_2$, $O_3$, $HNO_3$, and $C_2H_6$ were all included and continua for $H_2O$ and $CO_2$. Within 25 $cm^{-1}$ of line centres the Lorentz line shape formulation was used throughout. The criteria used to distinguish between line-by-line absorption and continuum absorption are described by *Edwards* [1987]. This should be borne in mind when comparing the computed absorptions split up into the individual components in Table 2. The frequency interval for the calculations was 0.05 $cm^{-1}$. The computed radiances were then averaged over 1 $cm^{-1}$ intervals and finally multiplied by the AVHRR NOAA 9 filter response functions and converted into brightness temperatures. It should be noted that the version of GENLN2 used here does not include aerosol absorption, so for this comparison the values computed by the band model were used. The sea surface emissivity was calculated as for the band model described in the previous section, so the top of the atmosphere radiance included a contribution from downwelling reflected radiation, which was specularly reflected at the sea surface.

## 3. Model Comparisons

### 3.1. *Standard Atmospheres*

The satellite brightness temperatures for a set of three standard atmospheres have been calculated for each of the models. The atmospheres used were the tropical, mid-latitude summer and mid-latitude winter of *McClatchey et al.* [1972]. Filter profiles for the three infrared channels of the AVHRR instrument on the NOAA 9 satellite were used, and the brightness temperatures for zenith angles of 0° and 50° were compiled. Initial comparisons were made in terms of temperature deficits (surface temperatures minus brightness temperatures), as they are a simple indication of the magnitude of the effect of atmospheric absorption. The results are shown in Table 1.

For the 3.7-μm channel the band model generally gives slightly smaller deficits than the other three models, with the effect being most obvious for the tropical atmosphere. The line-by-line and LOWTRAN models show good agreement, with the only significant difference being the slightly larger deficit in the line-by-line model for the tropical atmosphere. GENLN2 gives somewhat higher deficits for the mid-latitude atmospheres.

For all atmospheres the LOWTRAN deficits for the 10.8-μm channel are larger than those for the other models. The band model deficits are marginally larger than those for the line-by-line model. GENLN2 deficits are slightly smaller, except for the winter profile, where the deficits are much smaller. At 12.0 μm the LOWTRAN deficits are again the largest, while the line-by-line and band models give excellent agreement. The GENLN2 deficits are smaller, especially for the winter profile.

For more detailed comparisons the three models have been used with the tropical atmosphere and a zenith angle of 0° to assess the effect of the various components contributing to the deficits. The results are shown in Table 2. The values given for the emissivity are obtained by removing all of the absorbers and then calculating the effect of including emissivity. This different approach is necessary, as there is interaction between the absorption and emissivity contributions due to the surface reflection of downwelling radiation. The analysis shows that the difference between the band and LOWTRAN models at 3.7 μm is mainly due to the aerosol component. The water vapor contributions are similar, and the mixed gas absorption is slightly larger in the band model and much larger in the GENLN2 results.

For the 10.8- and 12.0-μm channels the discrete component analysis shows that there are only small differences across the models for a particular component. In particular, the con-

TABLE 2*a*. Discrete Component Analysis of Absorption in the 3.7-$\mu$m Channel for the Tropical Atmosphere

| Model | LWT | LBL | BND | GL2 |
|---|---|---|---|---|
| Normal | 3.54 | 3.64 | 3.23 | 3.42* |
| Normal-continuum | 3.21 (0.33) | 2.65 (0.99) | 2.87 (0.36) | 3.10*(0.32) |
| Normal-water lines | 2.05 (1.49) | 2.52 (1.12) | 1.75 (1.48) | 2.03*(1.39) |
| Normal-mixed gases | 3.15 (0.39) | 2.99 (0.65) | 2.71 (0.52) | 2.50*(0.92) |
| Normal-aerosols | 3.06 (0.48) | 3.46 (0.18) | 3.05 (0.18) | 3.24*(0.18) |
| Emissivity | (0.65) | (0.65) | (0.65) | (0.65) |
| Totals | 3.34 | 3.59 | 3.19 | 3.46 |

LWT, LOWTRAN; LBL, line-by-line; BND, spectral band; GL2, GENLN2. The values in parentheses are the contributions for each discrete component.

*A deficit of 0.18 K for 50° (the BND model values) was added for aerosols. No aerosols were included for the 10.8- and 12.0-$\mu$m channels.

tinuum contribution to the deficit in the LOWTRAN and band models are similar for the 12.0-$\mu$m channel, since the coefficients used are essentially the same; while in the 10.8-$\mu$m channel the LOWTRAN continuum deficit is less, since the absorption coefficient has been modified. In the case of the water vapor lines, the LOWTRAN deficits are less than for the band model. The 12.0-$\mu$m channel deficits due to water vapor lines and mixed gases are significantly higher for GENLN2.

There is one interesting aspect of the values given in Table 2. As the different absorption processes are independent and are relatively weak, it is expected that the sum of the individual deficits should be similar to the total deficit. This is seen to be so for all cases, except for the LOWTRAN model, where, for the 10.8- and 12.0-$\mu$m channels, the sum of the components contributing to the deficit is considerably less than the total deficit. Further analysis was undertaken to determine the source of this large difference. Analysis, as described earlier, was again used, but with pairs of components removed instead of single components. By removing the two components together, any interactions between the various components can be determined; that is, checking this difference with that derived after summing the corresponding separate differences for the same two components given in Table 2 would reveal that an interaction is occurring between those two components. Table 3 gives the results, which show a significant contribution from an interaction between the water lines and the continuum in both channels, while a contribution is evident from a mixed gases–continuum interaction in the 10.8-$\mu$m channel. For the mid-latitude summer atmosphere the difference in the total temperature deficit and the sum of individual components making up the deficit is not as great as with the tropical model. This arises because the continuum absorption is much less, and consequently a smaller interaction between the components has resulted. Hence it is concluded that the interaction appearing in LOWTRAN is a function of the strength of the continuum absorption.

### 3.2. *Coincident Radiosonde and Satellite Data*

During 1984 and 1985 a set of ship-based radiosonde data was obtained, with coincident satellite brightness temperatures for clear-sky views of the sea surface. Sea surface temperatures were measured using bucket thermometers and a ship-borne infrared radiometer. The data collected in 1984 were for the mid-latitudes off the southeast coast of Australia and include NOAA 7 imagery. The remainder of the data were collected in the Coral Sea, with the satellite data coming from the NOAA 9 satellite. Details of the data are given in Table 4.

The band model is used to calculate the brightness temperatures expected at the satellite for each of the 14 occasions listed in Table 4. The vertical profiles of temperature and water vapor content were obtained from the radiosonde data, and the surface temperature taken was that measured with an infrared radiometer. When there were no radiometer data available, the bucket temperature was used. In these latter cases, care was taken to ensure that the temperature was representative of the surface mixed layer and that no near-surface temperature gradients were present. The band transmission model was first used to determine the downcoming sky radiance at the surface, and this was used to correct the radiometer brightness temperature for nonunity surface emissivity and thus give a true (blackbody) radiative temperature for the sea surface. In all cases this correction was between 0.5 and 0.8 K. The calculated brightness temperatures and the satellite data are included in Table 4.

The model-derived and measured temperature deficits are compared in Figure 1, which also includes the earlier results of

TABLE 2*b*. Discrete Component Analysis of Absorption in the 10.8-$\mu$m Channel for the Tropical Atmosphere

| Model | LWT | LBL | BND | GL2 |
|---|---|---|---|---|
| Normal | 4.83 (0.00) | 4.13 (0.00) | 4.29 (0.00) | 3.95 (0.00) |
| Normal-continuum | 2.56 (2.27) | 1.82 (2.31) | 1.87 (2.42) | 1.62 (2.33) |
| Normal-water lines | 4.24 (0.59) | 3.46 (0.67) | 3.62 (0.67) | 3.21 (0.74) |
| Normal-mixed gases | 4.43 (0.40) | 3.84 (0.29) | 3.81 (0.48) | 3.56 (0.39) |
| Normal-aerosol | 4.83 (0.03) | 4.08 (0.05) | 4.23 (0.06) | no aerosols |
| Normal-ozone | 4.74 (0.09) | . . . | . . . | . . . |
| Emissivity | (0.62) | (0.66) | (0.52) | (0.52) |
| Totals | 4.00 | 3.98 | 4.15 | 3.98 |

LWT, LOWTRAN; LBL, line-by-line; BND, spectral band; GL2, GENLN2. Values in parentheses as in Table 2*a*.

TABLE 2c. Discrete Component Analysis of Absorption in the 12.0-μm Channel for the Tropical Atmosphere

| Model | LWT | LBL | BND | GL2 |
|---|---|---|---|---|
| Normal | 5.95 (0.00) | 5.72 (0.00) | 5.67 (0.00) | 5.55 (0.00) |
| Normal-continuum | 2.76 (3.19) | 2.79 (2.93) | 2.55 (3.12) | 2.48 (3.07) |
| Normal-water lines | 4.73 (1.22) | 4.36 (1.36) | 4.33 (1.34) | 4.04 (1.51) |
| Normal-mixed gases | 5.86 (0.09) | 5.63 (0.09) | 5.56 (0.11) | 5.39 (0.16) |
| Normal-aerosol | 5.95 (0.00) | 5.68 (0.04) | 5.59 (0.08) | no aerosols |
| Emissivity | (0.60) | (1.02) | (0.79) | (0.79) |
| Totals | 5.10 | 5.44 | 5.44 | 5.53 |

LWT, LOWTRAN; LBL, line-by-line; BND, spectral band; GL2, GENLN2. Values in parentheses as in Table 2a.

*Barton* [1985]. The new data, which include measurements in tropical regions, confirm the earlier conclusion that the model tends to underestimate the deficit in both of the split-window channels of the AVHRR. The implications of this disparity are discussed by *Barton* [1985]. For both sets of data, the band model shows that an increase of 25% in the water vapor continuum absorption is sufficient to give good agreement between the model and satellite measurements. Nevertheless, *Barton* [1985] shows that there is very close agreement, over a large range of deficits, between the model-derived SST algorithm and the MCSST operational algorithm derived by *McClain et al.* [1985] from a regression analysis of satellite brightness temperatures and collocated buoy data. An alternative cause of this discrepancy between measured and model-derived deficits has recently been proposed by *Cutten* [1989]. He suggests that the extra absorption evident in the satellite measurements may be due to invisible layers of ice-supersaturated particles in the middle troposphere (generally referred to as subvisual cirrus).

The intercomparion of the four transmission models shows that they all give similar results for the standard atmospheres used. The major errors appear to be due to the uncertainty in the absorption coefficients and in the absorption mechanism. The remainder of this paper concentrates on the theoretical derivation of SST algorithms for the AVHRR and ATSR instruments using the spectral band model. This model is used, because its performance is similar to the other three, it is computationally quicker, and it accurately reproduces the operational MCSST algorithm [*Barton*, 1985]. For the AVHRR and ATSR instruments an intercomparison between several different forms of algorithm is given, along with predictions for the absolute SST accuracy available from the ATSR data.

## 4. Theoretical Algorithms

Here in a general form the sea surface temperature is expressed as a linear combination of the satellite brightness temperatures and the water vapor column; namely,

$$\mathrm{SST} = a_0 + \sum_k a_k T_k + a_w W \qquad k = 1 \cdots 6 \tag{1}$$

where $a_0$, $a_k$, and $a_w$ are coefficients to be determined, $W$ is the vertical water vapor column, and $T_k$ are the satellite-measured brightness temperatures. The coefficients $a_0$, $a_k$, and $a_w$ include a zenith angle ($\theta$) dependence such that

$$a_k = a_{0k} + a_{1k}(\sec\theta - 1) + a_{2k}(\sec\theta - 1)^2 + \cdots \tag{2}$$

In the case of the forward view of the ATSR, the values of $\theta$ used in the algorithm are those applicable to the nadir scan at the same pixel location.

For the AVHRR calculations, $k = 1, 2, 3$ refers to the infrared channels 3, 4, and 5, centered at 3.7, 10.8, and 12.0 μm, and the water vapor column is not included. Either a pair of channels or all three can be included in the algorithm.

For ATSR, $k = 1, 2, 3$ refers to the 3.7-, 10.8-, and 12.0-μm channels (similar to the AVHRR channels) in the nadir scan, and $k = 4, 5, 6$ refers to the same three channels in the forward looking scan. For the ATSR nadir scan the zenith angle at the Earth's surface varies from zero at the subsatellite point to approximately 20° at the edge of the swath, while for the forward scan the angle varies from 55° on the subsatellite track to 52° at the swath edge. The water vapor column beneath the satellite is obtained from the nadir-pointing dual-channel passive microwave radiometer that is an important component of the ATSR.

For both the AVHRR and the ATSR, the noise associated with the measurement in each channel, including that pertaining to $W$, is included in the theoretical derivation of the SST algorithms. The noise in the different channels is assumed to be uncorrelated. The algorithms are derived by minimizing a cost function, which reduces to

$$\sigma^2 = (1/N)\sum_1^N \left[\mathrm{SST} - a_0 - \sum_1^6 a_k T_k - a_w W\right]^2 + \sum_1^6 (a_k\sigma_k)^2 + (a_w\sigma_w)^2 \tag{3}$$

in the special case where zenith angle dependence is not included in the coefficients $a_k$. Here $N$ is the number of data points (i.e., radiosonde profiles), $\sigma_k$ is the noise equivalent temperature in channel $k$, and $\sigma_w$ is the error associated with the water vapor column determination. In (3), $\sigma$ is then a measure of the rms error in the derivation of SST, using satellite data. In the following work the band model was used with a set of

TABLE 3. Component-Pair Analysis for the LOWTRAN 6 Model of Absorption in the Three Channels for the Tropical Atmosphere

| | Channel, μm | Deficit, K | Difference, K | Sum of Individual Component Differences |
|---|---|---|---|---|
| Normal-(continuum + water lines) | 3.7 | 1.67 | 1.87 | 1.82 |
| | 10.8 | 1.71 | 3.12 | 2.86 |
| | 12.0 | 0.98 | 4.97 | 4.41 |
| Normal-(continuum + mixed gases) | 3.7 | 2.80 | 0.74 | 0.72 |
| | 10.8 | 1.83 | 3.00 | 2.67 |
| | 12.0 | 2.67 | 3.28 | 3.28 |
| Normal-(water lines + mixed gases | 3.7 | 1.65 | 1.89 | 1.88 |
| | 10.8 | 3.81 | 1.02 | 0.99 |
| | 12.0 | 4.63 | 1.32 | 1.31 |

TABLE 4. Details of Ship, Radiosonde, and Satellite Data Used in Comparison With Spectral Band Model

| Date | Local Time | Latitude, °S | Longitude, °E | Bucket Temperature | Radiometer Temperature | Water Vapor, cm | Zenith Angle, deg | Satellite Temperatures | | Model Temperatures | |
|---|---|---|---|---|---|---|---|---|---|---|---|
| | | | | | | | | T4 | T5 | T4 | T5 |
| | | | | | *Mid-latitude* | | | | | | |
| July 5, 1984 | 1645 | 40.77 | 147.92 | 12.0 | 12.6 | 1.20 | 33 | 9.6 | 8.7 | 10.3 | 9.5 |
| Aug. 8, 1984 | 0350 | 34.88 | 151.22 | 18.0 | 18.0 | 1.24 | 59 | 13.7 | 12.1 | 13.9 | 12.6 |
| Aug. 8, 1984 | 1615 | 36.57 | 150.35 | 15.6 | 15.2 | 1.34 | 27 | 13.6 | 12.6 | 13.3 | 12.7 |
| Oct. 7, 1984 | 1542 | 32.90 | 153.53 | 20.7 | ··· | 1.73 | 16 | 17.5 | 16.2 | 17.9 | 16.7 |
| Oct. 12, 1984 | 1621 | 31.58 | 153.90 | 20.3 | ··· | 1.80 | 46 | 18.1 | 17.1 | 17.9 | 17.1 |
| Oct. 13, 1984 | 0345 | 31.75 | 153.18 | 21.2 | ··· | 1.91 | 49 | 18.0 | 17.0 | 18.4 | 17.7 |
| Dec. 1, 1984 | 1700 | 38.80 | 148.33 | 16.4 | 16.1 | 1.37 | 26 | 14.6 | 13.6 | 14.3 | 13.7 |
| Dec. 2, 1984 | 0420 | 38.67 | 148.12 | 15.0 | 15.0 | 1.39 | 3 | 13.5 | 12.9 | 13.7 | 13.3 |
| | | | | | *Tropical* | | | | | | |
| Oct. 25, 1985 | 1346 | 18.42 | 153.50 | 26.7 | 26.7 | 4.23 | 50 | 19.9 | 17.7 | 20.3 | 18.7 |
| Oct. 28, 1985 | 1453 | 15.57 | 156.53 | 28.4 | 28.4 | 4.05 | 65 | 15.6 | 12.5 | 17.3 | 14.6 |
| Oct. 29, 1985 | 1443 | 13.37 | 154.93 | 29.1 | 29.2 | 4.18 | 54 | 19.1 | 16.0 | 20.3 | 17.8 |
| Oct. 31, 1985 | 0157 | 13.03 | 151.73 | 27.4 | 27.3 | 3.09 | 36 | 22.9 | 21.4 | 22.9 | 21.6 |
| Oct. 31, 1985 | 1422 | 13.53 | 150.75 | 27.4 | 27.1 | 3.46 | 5 | 22.5 | 20.7 | 23.0 | 21.7 |
| Nov. 4, 1985 | 0255 | 16.57 | 147.68 | 26.6 | 26.9 | 5.10 | 43 | 17.9 | 15.1 | 18.3 | 15.8 |

Temperatures are given in degrees Celsius.

74 radiosonde profiles to provide data sets of SST and related satellite brightness temperatures. The profiles cover a large range of climates but have a bias to maritime and tropical locations. Further details of the minimization procedure and the formulation of the problem to allow coefficients which depend upon $\theta$ are given in the appendix.

### 4.1. *AVHRR*

In this section the filter response functions for the NOAA 9 instrument are used with the band model to produce theoretical brightness temperatures for zenith angles of 0°, 30°, 40°, 50°, 55°, and 60°, and these are considered to be adequate for producing algorithms that are applicable across the entire

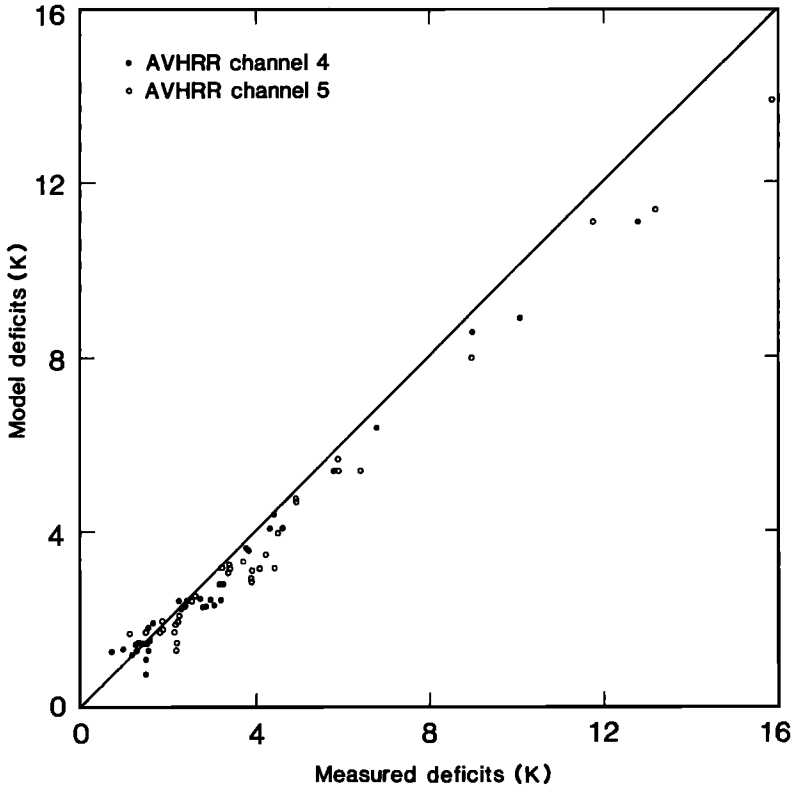


Fig. 1. Comparison between measured temperature deficits (ship SST minus satellite brightness temperature) and those computed using the band model.

TABLE 5. Coefficients for AVHRR SST Algorithms

| AVHRR Channels | NE$\delta$T | $a_{00}$ | $a_{1,0}$ | $a_{0,1}$ | $a_{1,1}$ | $a_{0,2}$ | $a_{1,2}$ | $a_{0,3}$ | $a_{1,3}$ | $\sigma$ |
|---|---|---|---|---|---|---|---|---|---|---|
| 4,5 | 0 | 2.64 | −2.36 | 0 | 0 | 3.709 | 0.839 | −2.717 | −0.830 | 0.322 |
| 4,5 | 0.05 | 1.38 | −2.17 | 0 | 0 | 3.637 | 0.844 | −2.640 | −0.835 | 0.411 |
| 4,5 | 0.10 | −2.07 | −1.70 | 0 | 0 | 3.439 | 0.853 | −2.429 | −0.845 | 0.591 |
| 4,5 | 0.15 | −6.93 | −1.20 | 0 | 0 | 3.160 | 0.854 | −2.132 | −0.848 | 0.781 |
| 3,4 | 0 | −9.85 | −2.00 | 1.466 | 0.070 | −0.423 | −0.057 | 0 | 0 | 0.195 |
| 3,4 | 0.10 | −10.51 | −1.80 | 1.439 | 0.083 | −0.395 | −0.071 | 0 | 0 | 0.249 |
| 3,4,5 | 0 | −4.43 | −2.66 | 0.908 | 0.184 | 1.191 | −0.140 | −1.079 | −0.030 | 0.128 |
| 3,4,5 | 0.10 | −7.15 | −1.66 | 1.161 | 0.076 | 0.440 | 0.000 | −0.569 | −0.164 | 0.202 |
| 4,5* | 0.10 | 0.71 | 0 | 0 | 0 | 3.703 | 0 | −2.704 | 0 | 0.490 |
| 4,5† | 0 | 4.15 | 0 | 0 | 0 | 3.909 | 0 | −2.921 | 0 | 0.269 |
| 4,5† | 0.10 | −0.46 | 0 | 0 | 0 | 3.638 | 0 | −2.634 | 0 | 0.540 |

Subscripts 1, 2 and 3 refer to channels 3, 4, and 5, respectively. The form of the algorithms is given in equations (2) and (3).
*MCSST coefficients for E.P. McClain's (private communication, 1986) night-time algorithm.
†These algorithms are determined using data for angles of 0°, 30°, and 40° only, with no angular dependence for the coefficients.

AVHRR swath. The final algorithms were tested at other angles to confirm there was no instability in the determination of the coefficients.

The results of using the least squares minimization procedure are given in Table 5. The first four sets of coefficients show that there is considerable variation in the magnitude of the coefficients, depending on the noise temperature ($NE\delta T$) of the AVHRR channels. Assuming a noise temperature of 0.1 K (*Lauritson et al.* [1979] state that $NE\delta T < 0.12$ K), an algorithm using channels 4 and 5 for the entire swath of the AVHRR gives a satellite-derived SST with an accuracy of 0.6 K.

Table 5 also shows that the AVHRR instrument may be able to give an SST with an accuracy better than 0.5 K if either channels 3 and 4, or 3, 4, and 5, are used. Channel 3 is affected by reflected solar radiation, and so this measurement is either restricted to nighttime or to areas where the amount of solar contamination can be assessed. Unfortunately, SSTs with this accuracy are yet to be obtained from the AVHRR as, in the past, the AVHRR channel 3 data have been somewhat noisy, and this has limited their use in accurate SST determination. Attempts have been made to reduce this noise in the latest AVHRR instruments, and future MCSST algorithms may use the 3.7-$\mu$m channel for the operational derivation of SST.

The last two sets of coefficients in Table 5 are determined for comparison with the NOAA 9 MCSST algorithm that uses AVHRR data with zenith angles less than 45° and does not include any zenith angle dependence (E. P. McClain, private communication, 1986). When typical values of brightness temperatures are considered, the theoretical algorithm gives an SST that is 0.2 K higher than that from the MCSST algorithm over a wide range of values. The analysis also confirms the inference of *McClain* [1981] that for zenith angles less than 45° it is not necessary to incorporate any angular dependence in the AVHRR SST algorithms.

*Barton* [1985] evaluated two-channel algorithms in which the coefficient $a_{k+1}$ was set equal to $a_{k-1}$ and used three angular basis functions for including the effects of different zenith angles. These functions were 1, (sec $\theta$ − 1) and (sec $\theta$ − 1)$^2$. In this work we remove the former constraint imposed on the coefficients and use only the first two angular basis functions. The results given in Table 6 indicate that for noise temperatures of 0.1 K, the inclusion of the third function only gives a marginal improvement in the SST accuracy over the entire AVHRR swath. Similar results are found for the case when the noise temperatures in the satellite data are set to zero.

### 4.2. *ATSR*

The ATSR uses a conically scanning objective mirror to provide two views across the subsatellite track, one in the nadir and one forward of the satellite. The zenith angle at the Earth's surface and the across- and along-track distances from the subsatellite point for a selection of ATSR pixels are given in Table 7. As in the AVHRR case, the filter response functions for the NOAA 9 instrument were used to simulate the brightness temperatures to be measured by the ATSR. These temperatures were calculated using the spectral band model for the pixels, given in Table 7.

The minimization procedure was applied to various selections of channels in both views to provide SST algorithms for the ATSR instrument. The derived coefficients for the algorithms are given in Table 8. Each selection of infrared channels is treated with and without the water vapor column that is provided by the microwave channels. In all cases the noise temperature for each of the infrared channels was assumed to be 0.04 K, and the error in the water vapor measurement assumed to be 0.4 gm cm$^{-2}$.

TABLE 6. Coefficients for SST Algorithms for AVHRR Instrument, using either 1, 2, or 3 Angular Basis Functions

| AVHRR Channels | $a_{0,0}$ | $a_{1,0}$ | $a_{2,0}$ | $a_{0,2}$ | $a_{1,2}$ | $a_{2,2}$ | $a_{0,3}$ | $a_{1,3}$ | $a_{2,3}$ | $\sigma$ |
|---|---|---|---|---|---|---|---|---|---|---|
| 4,5 | 7.42 | 0 | 0 | 4.166 | 0 | 0 | −3.190 | 0 | 0 | 0.7916 |
| 4,5 | −2.07 | −1.70 | 0 | 3.439 | 0.853 | 0 | −2.429 | −0.845 | 0 | 0.5914 |
| 4,5 | −2.45 | 4.80 | −7.71 | 3.419 | 1.118 | −0.304 | −2.407 | −1.136 | 0.333 | 0.5904 |

See the text for details. In all cases the $NE\delta T$ for each channel was set at 0.10 K. Subscripts as in Table 5.

TABLE 7. Along- and Across-Track Distances and Zenith Angles for Pixels Used in ATSR Algorithm Development

| Nominal Across-Track Distance, km | Nadir View | | | Forward View | | |
|---|---|---|---|---|---|---|
| | Across-Track Distance, km | Along-Track Distance, km | Zenith Angle, deg | Across-Track Distance, km | Along-Track Distance, km | Zenith Angle, deg |
| 0 | 0 | 0 | 0 | 0 | 901.2 | 55.00 |
| 50 | 50.4 | 3.8 | 4.17 | 50.6 | 897.3 | 54.91 |
| 100 | 100.2 | 15.1 | 8.33 | 100.1 | 885.7 | 54.64 |
| 150 | 149.6 | 34.6 | 12.53 | 149.0 | 866.1 | 54.20 |
| 200 | 200.4 | 64.3 | 16.98 | 200.0 | 835.7 | 53.46 |
| 250 | 250.1 | 105.4 | 21.55 | 250.4 | 793.2 | 52.40 |

The first six algorithms in Table 8 are for daytime use, that is, the 3.7-$\mu$m channel data are not used because of contamination by reflected solar radiation. The first algorithm using the split-window channels at 10.8 and 12.0 $\mu$m in the nadir scan gives an SST error of 0.27 K. This improvement over the AVHRR equivalent algorithm (see Table 5) is due to the lower noise figures used and the smaller range of zenith angles (0°–22.15°). The second algorithm that incorporates the water vapor data shows no improvement over that without water vapor. This suggests that the additional water vapor information is redundant, and so the dual-channel data may be used to give a useful measure of water vapor content. The next pair of algorithms are for the 10.8-$\mu$m channel only and use the nadir and forward views. Without the water vapor information the derived SST has the same accuracy as the split-window channels in the nadir. However, if the water vapor is included, the accuracy improves to 0.23 K. The last pair of daytime algorithms use all the infrared data available, that is, the 10.8- and 12.0-$\mu$m channels in both views, and show little improvement on the second combination of two infrared channels with water vapor included.

The nighttime algorithms all use the 3.7-$\mu$m channel and all perform better than the daytime algorithms because of the smaller water vapor absorption in this channel. The dual-window channels (10.8 and 3.7 $\mu$m) in the nadir scan give an SST error of 0.16 K. As for the daytime split-window algorithm, there is no improvement in including the water vapor information. By combining the forward and nadir views in the 3.7-$\mu$m channel, an error of 0.19 K is obtained, and there is some improvement if the water vapor are included. By using the dual view and the multichannel capability of the ATSR, the theoretical algorithms for nighttime can reproduce the SST with an rms error near 0.09 K. In these cases, little improvement is gained by including the water vapor data.

## 5. Concluding Remarks

The intercomparison of the four atmospheric transmission models shows good agreement in the calculated satellite brightness temperatures in the two infrared spectral widows used for SST measurement. The major errors between the calculations and satellite measurements could result from a poor knowledge of water vapor absorption coefficients and aerosol profiles. Both horizontal path and laboratory experiments indicate that the continuum absorption coefficients used here are too large, while comparison of satellite data with transmission models using aerological data suggests that the coefficients are too small. This conflict between the measurements is compounded by the uncertainty of whether the continuum "anomalous" absorption is due to water vapor dimers, to the wings of (spectrally) distant lines, or to some other mechanism.

In spite of this poor understanding of the water vapor absorption coefficients, the models can be used to develop reasonably accurate multichannel SST algorithms [*Barton*, 1985], at least in the split-window region between 10 and 13 $\mu$m. That algorithms using the 3.7-$\mu$m channel have not been developed with the same confidence is mainly due to the noisy 3.7-$\mu$m data supplied by past AVHRR instruments. Also, there has been a lack of laboratory and ground-based absorption measurements at 3.7 $\mu$m.

In this paper the simpler and computationally faster band model is used to develop AVHRR and ATSR algorithms. As with the AVHRR MCSST algorithms, those determined prelaunch for the ATSR will probably need some fine tuning to give more accurate SSTs. However, the theoretical algorithms will allow the development of a measurement and analysis strategy to gain the maximum value from future satellite data.

The algorithms derived in this work show that the effects of variable water vapor and temperature can be accounted for and an accurate SST derived from satellite data. However, while the model uses a set of radiosonde profiles for input data, it also assumes (1) a constant aerosol distribution in the lower troposphere, (2) no stratospheric aerosols and no minor atmospheric constituents, (3) no variations in ozone amount, and (4) standard values for stratospheric temperature profiles above the highest radiosonde level. In the past, major changes in the stratospheric aerosol content have resulted in the modification of operational SST algorithms [*Walton*, 1985]. Thus further development of the SST algorithms with a set of atmospheric profiles that includes realistic variations in ozone content, stratospheric aerosol concentrations, and stratospheric temperatures is required. As the nature of the stratosphere is continually changing, it may also be necessary to consider extra minor constituents that absorb in the thermal infrared, for example, chlorofluorocarbons.

The multiwavelength approach is useful for determining the effects of varying water vapor amounts but is not sensitive to the effects of other atmospheric constituents, unless their relative absorption at the different wavelengths is similar to that of water vapor. The dual-angle technique can account for absorption variations due to the different concentrations in all absorbing species. It is in this regard that the dual-angle approach of the ATSR is expected to give a significant improvement in SST accuracy.

The accuracies of the different ATSR algorithms given in Table 8 have all been obtained with "ideal" conditions; that is,

TABLE 8. Coefficients of SST Algorithms for ATSR Instrument

| ATSR Channels | Water Vapor | $a_{0,0}$ | $a_{1,0}$ | $a_{0,1}$ | $a_{1,1}$ | $a_{0,2}$ | $a_{1,2}$ | $a_{0,3}$ | $a_{1,3}$ | $a_{0,4}$ | $a_{1,4}$ | $a_{0,5}$ | $a_{1,5}$ | $a_{0,6}$ | $a_{1,6}$ | $a_{0,w}$ | $a_{1,w}$ | $\sigma$ |
|---|---|---|---|---|---|---|---|---|---|---|---|---|---|---|---|---|---|---|
| | | | | | | | | | *Daytime* | | | | | | | | | |
| 2,3 | no | 1.50 | 3.86 | 0 | 0 | 3.668 | 0.809 | −2.672 | −0.822 | 0 | 0 | 0 | 0 | 0 | 0 | 0 | 0 | 0.2674 |
| 2,3 | yes | 1.71 | 3.87 | 0 | 0 | 3.603 | 0.804 | −2.607 | −0.817 | 0 | 0 | 0 | 0 | 0 | 0 | 0.030 | 0.014 | 0.2668 |
| 2,5 | no | −4.11 | −14.13 | 0 | 0 | 3.427 | 10.521 | 0 | 0 | 0 | 0 | −2.418 | −10.47 | 0 | 0 | 0 | 0 | 0.2632 |
| 2,5 | yes | −1.80 | 0.05 | 0 | 0 | 3.121 | 7.730 | 0 | 0 | 0 | 0 | −2.119 | −7.725 | 0 | 0 | 0.166 | 0.803 | 0.2263 |
| 2,3,5,6 | no | −1.56 | 12.48 | 0 | 0 | 3.325 | 0.974 | −0.926 | −0.212 | 0 | 0 | −1.188 | 4.076 | −0.208 | −4.872 | 0 | 0. | 0.2300 |
| 2,3,5,6 | yes | −1.28 | 12.07 | 0 | 0 | 3.004 | 2.668 | −0.245 | −1.785 | 0 | 0 | −1.572 | 4.405 | −0.185 | −5.317 | 0.145 | −0.335 | 0.2167 |
| | | | | | | | | | *Nighttime* | | | | | | | | | |
| 1,2 | no | −9.37 | −3.25 | 1.491 | −0.055 | −0.450 | 0.071 | 0 | 0 | 0 | 0 | 0 | 0 | 0 | 0 | 0 | 0 | 0.1605 |
| 1,2 | yes | −9.31 | −4.18 | 1.487 | 0.010 | −0.446 | 0.009 | 0 | 0 | 0 | 0 | 0 | 0 | 0 | 0 | 0.004 | −0.056 | 0.1605 |
| 1,4 | no | −6.50 | −31.45 | 3.087 | 4.594 | 0 | 0 | 0 | 0 | −2.065 | −4.466 | 0 | 0 | 0 | 0 | 0 | 0 | 0.1905 |
| 1,4 | yes | −4.07 | −15.27 | 2.646 | 2.667 | 0 | 0 | 0 | 0 | −1.631 | −2.598 | 0 | 0 | 0 | 0 | 0.122 | 0.383 | 0.1517 |
| 1,2,4,5 | no | −6.30 | −9.07 | 1.324 | 0.487 | 0.805 | 0.768 | 0 | 0 | −0.341 | 0.616 | −0.764 | −1.822 | 0 | 0 | 0 | 0 | 0.0994 |
| 1,2,4,5 | yes | −5.45 | −12.79 | 1.341 | 0.457 | 0.850 | 0.709 | 0 | 0 | −0.414 | 0.874 | −0.755 | −1.976 | 0 | 0 | 0.042 | −0.175 | 0.0969 |
| 1,2,3,4,5,6 | no | −5.32 | −0.89 | 1.203 | −0.859 | 0.667 | 0.487 | −0.158 | 0.389 | −0.256 | 0.980 | −0.152 | 0.776 | −0.283 | −1.760 | 0 | 0 | 0.0840 |
| 1,2,3,4,5,6 | yes | −5.32 | −3.59 | 1.198 | −0.936 | 0.663 | 0.567 | −0.174 | 0.095 | −0.248 | 1.180 | −0.133 | 0.938 | −0.284 | −1.820 | −0.001 | −0.248 | 0.0838 |

Channels 1, 2, and 3 refer to 3.7, 10.8, and 12.0 μm in the nadir scan and 4, 5, and 6 refer to the same three wavelengths in the forward scan. Subscripts as in Table 5.

the only atmospheric variables used in their derivation have been tropospheric water vapor and temperature profiles. For the "real" atmosphere case, in which all the extra absorption variables mentioned earlier are included, the rms errors of SST measurement will obviously become larger. The daytime algorithms show a similar error for the split-window algorithm and the dual-view algorithm of near 0.25 K. With more realistic atmospheric profiles, including variations in aerosol content, the final operational SST accuracy should be near the planned 0.3 K. For the nighttime algorithms the calculated noise figures of less than 0.1 K will probably increase to near 0.2 K for the operational algorithms: still less than the planned ATSR performance.

The ATSR algorithm analysis shows that the inclusion of an independent water vapor column measurement from microwave channels can significantly improve the accuracy of SST determination using the dual-view technique at one wavelength, but helps only marginally with the multiwavelength determination. As mentioned earlier, this analysis is performed under normal conditions with "well behaved" atmospheres. For abnormal profiles of temperature and water vapor, the inclusion of the two microwave brightness temperatures in the SST algorithm instead of a derived water vapor column is expected to give further improvements to the accuracy. A microwave transmission model will be implemented to investigate this possibility.

The effect of horizontal variations in the atmosphere and the effects of combining a larger forward pixel with a smaller nadir scan pixel still needs further evaluation. Finally, the detection of clouds, including subvisual cirrus, and aerosols (haze) in the field of view of the instrument is still a major problem. Methods of cloud detection, and the estimation of the errors introduced by undetected clouds, will require more study before the launch of the ERS 1 satellite in 1990.

## APPENDIX: THE MINIMIZATION PROCEDURE

The SST algorithms presented in this paper have the form

$$T = \sum_{0}^{k-1} a_k(\theta) C_k$$

where. (1) $\theta$ is the zenith angle in the nadir scan of the path from pixel to radiometer; (2) $C_0$ is a fictitious channel, with $C_0 = 1$, introduced for notational convenience; (3) $C_1, C_2, \cdots, C_{k-1}$ contain radiometric data.

This form is clearly appropriate for AVHRR, with $C_1$, $C_2$, and $C_3$ denoting the 3.7-, 10.8-, and 12.0-μm channels, respectively. For ATSR, where each pixel is observed twice, $C_1$, $C_2$, and $C_3$ denote the 3.7-, 10.8-, and 12.0-μm channels observed on the nadir scan, while $C_4$, $C_5$, and $C_6$ denote the same channels on the forward scan. In addition, $C_7$, $C_8$, $\cdots$ may denote microwave channels designed to monitor water vapor.

An alternative formulation for ATSR has the form

$$T = a_0(\theta) + \sum_{1}^{3} a_k(\theta) C_k(\theta) + \sum_{1}^{3} b_k(\theta') C_k(\theta') + \cdots,$$

where $\theta$ and $\theta'$ denote the zenith angles for the two observations of the pixel, and where $C_k(\theta)$ and $C_k(\theta')$ denote the corresponding radiometric data. However, because $\theta'$ can be expressed as a function of $\theta$,

$$\theta' = f(\theta)$$

so too can $b_k(\theta')$. Consequently, the alternative formulation can be reduced to the form assumed in this paper.

Each of the coefficients $a_k$ is assumed to be representable in terms of basis functions $f_l(\theta)$ as follows:

$$a_k(\theta) = \sum_0^{L-1} a_{lk} f_l(\theta)$$

In this paper the basis functions were chosen to be monomials in (sec $\theta - 1$),

$$f_l(\theta) = (\sec \theta - 1)^l, \qquad l = 0, 1, \cdots, L-1$$

With this formulation the task is to determine the coefficients $a_{lk}$ from a data set consisting of sea surface temperatures and predicted brightness temperatures, calculated for a number of model atmospheres and a number of zenith angles.

The atmospheres are labeled by an index $i = 0, 1, \cdots, I-1$, and the zenith angles are denoted by $\theta_j$, $j = 0, 1, \cdots, J-1$. The $L \times K$ matrix of parameters $a_{lk}$ is arranged into a column vector $\mathbf{x}$ with length $LK$, by defining

$$x_q = a_{lk}$$

where

$$q = l + kL \qquad \begin{matrix} l = 0, 1, \cdots, L-1 \\ k = 0, 1, \cdots, K-1 \end{matrix}$$

The atmosphere and angle labels are enumerated similarly by defining an index $p$, as follows,

$$p = j + iJ \qquad \begin{matrix} j = 0, 1, \cdots, J-1 \\ i = 0, 1, \cdots, I-1 \end{matrix}$$

The coefficients $a_{lk}$ must be chosen to solve, in some generalized sense, the set of linear equations,

$$y_p = \sum_0^{KL-1} A_{pq} x_q \qquad p = 0, 1, \cdots, IJ-1$$

where $A_{pq}$ denotes the product of the $l$th basis function, evaluated at zenith angle $\theta_j$, and the $k$th channel, evaluated with the $i$th model atmosphere and zenith angle $\theta_j$,

$$A_{pq} = f_l(\theta_j) C_k(i, \theta_j)$$

and $y_p$ denotes the true sea surface temperature,

$$y_p = T_i$$

a quantity which depends only on the atmosphere-ocean model and not on the zenith angle.

Noise in the temperature data leads to an error $\delta A$ in the matrix $A$. Since the mean and covariance of the instrumental noise are known for both AVHRR and ATSR, the coefficients $a_{lk}$ were chosen to minimise the expected value of the sum of squares of the model errors, given by

$$E^2 = \langle \|\mathbf{y} - (A + \delta A)\mathbf{x}\|^2 \rangle$$

where $\| \ \|$ denotes the $l_2$ norm. If the noise has zero mean, as assumed in this paper, then

$$\langle \delta A \rangle = 0$$

and a short calculation yields

$$E^2 = \|\mathbf{y} - A\mathbf{x}\|^2 \mathbf{x}^* B \mathbf{x}$$

where $B$ denotes the covariance matrix of the noise,

$$B = \langle \delta A^* \delta A \rangle$$

and the asterisk denotes the matrix transpose. It follows easily that

$$B_{qq'} = \sum_j f_l(\theta_j) f_{l'}(\theta_j) \sigma_k^2 \delta_{kk'}$$

The matrix $B$ is block diagonal and is singular, because the absence of noise in the fictitious channel 0 introduces a zero block into $B$. The singularity of $B$ influences the choice of algorithm to minimize $E^2$. The expression for $E^2$ can be reduced to

$$E^2 = \|\mathbf{y} - A\mathbf{x}\|^2 + \|H\mathbf{x}\|^2$$

where

$$H = Q^{1/2} P^*$$

and

$$B = PQP^*$$

is the singular value decomposition of $B$ [*Lawson and Hanson*, 1974].

Because $E^2$ can be written as the sum of squares of $IJ + KL$ functions, a *Levenberg* [1944]–*Marquardt* [1963] algorithm was used to find the coefficients $a_{lk}$, which minimize $E^2$. It was anticipated that linear constraints, both equality and inequality, might need to be imposed upon the coefficients $a_{lk}$, so the algorithm for nonlinear least squares with general linear constraints proposed by *Wright and Holt* [1985] was implemented on a personal computer. At each step of this algorithm, the problem is reduced to an unconstrained linear least squares problem in the subspace defined by the active constraints, which is solved using the Levenberg–Marquardt method. The desirability of leaving an active constraint is evaluated at each step. The length of each step is restricted to a circular region of trust about the current approximate minimizer, whose radius is updated according to the quality of the step after each iteration.

## REFERENCES


Barton, I. J., Dual-channel satellite measurements of sea surface temperature, *Q. J. R. Meteorol. Soc.*, *109*, 365–378, 1983.

Barton, I. J., Transmission model and ground-truth investigation of satellite-derived sea surface temperatures, *J. Clim. Appl. Meteorol.*, *24*, 508–516, 1985.

Ben-Shalom, A., B. Barzilai, D. Cabib, A. D. Devir, S. G. Lipson, and U.P. Oppenheim, Sky radiance at wavelengths between 7 and 14 μm: Measurement, calculation and comparison with LOWTRAN-4 predictions, *Appl. Opt.*, *19*, 838–839, 1980.

Burch, D. E., and R. L. Alt, Continuum absorption by $H_2O$ in the 700–1200 $cm^{-1}$ and 2400–2800 $cm^{-1}$ windows, *Rep. AFGL-TR-84-0128*, 32 pp., Air Force Geophys. Lab., Hanscom Air Force Base, Bedford, Mass., 1984.

Clough, S. A., F. X. Kneizys, E. P. Shettle, and G. P. Anderson, Atmospheric radiance and transmittance: FASCOD2, paper presented at 6th Conference on Atmospheric Radiation, Am. Meteorol. Soc., Williamsburg, Va., 1986.

Cutten, D. R., Atmospheric broadband transmission measurements and predictions in 8–13 μm window: Influence of water continuum absorption errors, *Appl. Opt.*, *24*, 1085–1087, 1985.

Cutten, D. R., Impact of ice-supersaturated layers on atmospheric radiance, *Infrared Millimeter Waves*, in press, 1989.

Deschamps, P. Y., and T. Phulpin, Atmospheric correction of infrared measurement of sea surface temperature using channels at 3.7, 11, and 12 μm, *Boundary Layer Meteorol.*, *18*, 131–143, 1980.

Edwards, D. P., GENLN2: The new Oxford line-by-line atmospheric transmission/radiance model, *Memo. 87.2*, Dep. of Atmos., Oceanic, and Planet. Phys., Univ. of Oxford, Oxford, England, 1987.

Edwards, D. P., Atmospheric transmittance and radiance calculations using line-by-line computer models, Critical Review of Technology,

Modelling of the Atmosphere, edited by L. S. Rothman, *Proc. Soc. Photo. Opt. Instrum. Eng., 928*, 94–116, 1988.

Kneizys, F. X., J. H. Chetwynd, R. W. Fenn, E. P. Shettle, L. W. Abreu, R. A. McClatchey, W. A. Gallery, and J. E. A. Selby, Atmospheric transmittance/radiance; Computer code LOWTRAN-5, *Rep. AFGL-TR-80-0067*, 233 pp., Air Force Geophys. Lab., Hanscom Air Force Base, Bedford, Mass., 1980.

Kneizys, F. X., J. H. Chetwynd, Jr., S. A. Clough, E. P. Shettle, L. W. Abreu, R. W. Fenn, W. O. Gallery, and J. E. A. Selby, Atmospheric transmittance/radiance: Computer code LOWTRAN 6, *Rep. AFGL-TR-83-0187*, Air Force Geophys. Lab., Hanscom 200 pp., Air Force Base, Bedford, Mass., 1983.

Lauritson, L., G. J. Nelson, and F. W. Porto, Data extraction and calibration of TIROS-N/NOAA radiometers, *NOAA Tech. Memo. NESS 107*, 73 pp., Natl. Oceanic and Atmos. Admin., U.S. Dept. of Commerce, Washington, D. C., 1979.

Lawson, C. L., and R. J. Hanson, Solving least squares problems, Prentice-Hall, Englewood Cliffs, N.J., 1974.

Levenberg, K., A method for the solution of certain non-linear problems in least squares, *Q. Appl. Math., 2*, 164–168, 1944.

Llewellyn-Jones, D. T., P. J. Minnett, R. W. Saunders, and A. M. Zavody, Satellite multi-channel infrared measurements of sea surface temperature of the N.E. Atlantic Ocean using AVHRR/2, *Q. J. R. Meteorol. Soc., 110*, 613–631, 1984.

McClain, E. P., Multiple atmospheric-window techniques for satellite-derived sea surface temperatures, in *Oceanography From Space*, edited by J. F. Gower, pp. 73–85, Plenum, New York, 1981.

McClain, E. P., W. G. Pichel, and C. C. Walton, Comparative performance of AVHRR-based multichannel sea surface temperatures. *J. Geophys. Res., 90*, 11,587–11,601, 1985.

McClatchey, R. A., R. W. Fenn, J. E. A. Selby, F. E. Volz, and J. S. Garing, Optical properties of the atmosphere, 3rd ed., *Rep. AFCRL-72-0497*, Air Force Cambridge Res. Lab., Bedford, Mass., 1972.

Marquardt, D. W., An algorithm for least-squares estimation of nonlinear parameters, *J. Soc. Ind. Appl. Math., 11*, 431–441, 1963.

Masuda, K., T. Takashima, and Y. Takayama, Emissivity of pure and sea waters for the model sea surface in the infrared window regions, *Remote Sens. Environ., 24*, 313–329, 1988.

Pontier, L., and C. Dechambenoy, Determination des constantes optiques de l'eau liquide entre 1 et 40 $\mu$m. Application an calcul de son pouroir et de son emissivite, *Ann. Geophys., 22*, 633–641, 1966.

Rothman, L. S., et al., The HITRAN database: 1986 edition, *Appl. Opt., 26*, 4058–4097, 1987.

Saunders, P. M., Aerial measurement of sea surface temperature in the infrared, *J. Geophys. Res., 72*, 4109–4117, 1967.

Saunders, P. M., Radiance of the sea and sky in the infrared window 800–1200 $cm^{-1}$, *J. Opt. Soc. Am., 58*, 645–652, 1968.

Saunders, R. W., and K. T. Kriebel, An improved method for detecting clear sky and cloudy radiances from AVHRR data, *Int. J. Remote Sens., 9*, 123–150, 1988.

Shettle, E., and R. W. Fenn, Models for the aerosols of the lower atmosphere and the effects of humidity variations on their optical properties, *Rep. AFGL-TR-79-0214*, 94 pp., Air Force Geophys. Lab., Bedford, Mass., 1979.

Walton, C., Satellite measurement of sea surface temperature in the presence of volcanic aerosols, *J. Clim. Appl. Meteorol., 24*, 501–507, 1985.

Weinreb, M. P., and M. L. Hill, Method to apply homogeneous-path transmittance models to inhomogeneous atmospheres, *J. Atmos. Sci., 30*, 662–666, 1980.

Wright, S. J., and J. N. Holt, Algorithms for nonlinear least squares with linear inequality constraints, *SIAM J. Sci. Stat. Comput., 6*, 1033–1048, 1985.

I. J. Barton and D. M. O'Brien, Division of Atmospheric Research, Commonwealth Scientific and Industrial Research Organisation, Private Bag No. 1, Mordialloc, Victoria 3195, Australia.

D. R. Cutten, Defence Science and Technology Organisation, P. O. Box 1650, Salisbury, South Australia, 5108, Australia.

D. T. Llewellyn-Jones and A. M. Zavody, Rutherford Appleton Laboratory, Chilton, Didcot, Oxford OX11 OQX, England.

R. W. Saunders, Meteorological Office Unit, Clarendon Laboratory, Parks Road, Oxford OX1 3PU, England.

(Received June 13, 1988;
revised November 17, 1988;
accepted November 28, 1988.)